Biophysical Journal, Volume *113*

Supplemental Information

Spatially Different Tissue-Scale Diffusivity Shapes ANGUSTIFOLIA3 Gradient in Growing Leaves

Kensuke Kawade, Hirokazu Tanimoto, Gorou Horiguchi, and Hirokazu Tsukaya

Supplemental Information

Spatially different tissue-scale diffusivity shapes ANGUSTIFOLIA3 gradient in growing leaves

Kensuke Kawade, Hirokazu Tanimoto, Gorou Horiguchi, Hirokazu Tsukaya

Contents

1. Supporting Materials and Methods

Mathematical models and simulations

(1) Tissue geometry and growth

We adopted a one-dimensional model to simulate the tissue-scale mobility of GFP in the square FRAP assay (Fig. S3) and AN3 gradient formation (Fig. S4) as differences in GFP mobility along the leaf medial-to-lateral axis were not significant (Figs. S1*C* and S1*D*). Cells were indexed from the leaf proximal part as 1, 2, …, *i*. We introduced parameter *j* to distinguish the number of cell divisions as 1, 2, …, *j*. Each cell had a length $L_{i;j,}$ and fluorescence intensity $F_{i;j}$, where *i* and *j* denoted the cell index and the number of cell divisions, respectively (Figs. S3 and S4).

The time span of GFP fluorescence recovery was from 0 to 45 min, so cell division would be negligible for simulation of tissue-scale GFP mobility in the square FRAP assay. In contrast, we implemented cell division for long-term simulation of the AN3 gradient formation (Fig. S4). Cells divide after each cell cycle, but kept their initial size by cell elongation, which promotes tissue growth. Protein concentration was distributed equally into the two daughter cells after cell division as;

$$F_{2i-1;j+1} = F_{2i;j+1} = F_{i;j}/2. \tag{S1}$$

(2) Protein diffusivity and degradation

Because the single-cell FRAP assay showed that intracellular movement of GFP was much more rapid than our observed timescale, we considered the GFP fluorescence intensity in a cell as a discrete and uniform single unit. Our single-cell FRAP assay revealed that protein movement through the plasmodesmata could be approximated as a pure diffusion process. The GFP influx into cell *i* in a given small time Δt, is thus described as a discrete event by;

$$\Delta C_i = \left\{ D_{i,i+1}\left(F_{i+1} - F_i\right) - D_{i-1,i}\left(F_i - F_{i-1}\right) \right\} \cdot \Delta t, \tag{S2}$$

where $D_{i\text{-}1,i}$ is a characteristic kinetic parameter of GFP diffusivity between cell *i-1* and *i*, which was determined by the single-cell FRAP assay (Figs. S3 and S4). We omitted the cell cycle index *j* to simplify the notation. With a position-independent kinetic rate of linear protein degradation k_{deg}, time-evolution of the protein concentration in the cell *i* is expressed as;

$$\Delta C_i = \left\{ D_{i,i+1}\left(F_{i+1} - F_i\right) - D_{i-1,i}\left(F_i - F_{i-1}\right) - k_{\deg} \cdot F_i \right\} \cdot \Delta t, \tag{S3}$$

which was solved with $\Delta t = 0.1$ sec for a total of 2^{16} steps (= 6553.6 sec) (Fig. S3).

(3) Parameters

Our simulation included the three parameters; cell length, and GFP diffusivity and degradation (Figs. S3 and S4). Cell length was estimated from the pictures used for the square FRAP assay (Fig. 3B; Fig. S2*D*). The kinetic parameter for GFP diffusivity ($D_{i\text{-}1,i}$) was determined by the single-cell FRAP assay. Because GFP fluorescence intensity in non-photobleached cells was almost constant in time in the single-cell FRAP assay (Fig. S2*B*), the characteristic time constant of the exponential recovery of GFP in a cell *i* (τ) and kinetic parameters $D_{i\text{-}1,i}$ and $D_{i,i+1}$ were related as;

$$D_{i-1,i} + D_{i,i+1} = 1/\tau. \tag{S4}$$

Given that the recovery kinetics of the single-cell FRAP assay exhibited weak position

dependency in the leaf primordia, there was little difference in the diffusion parameters between neighboring cells ($D_{i-1,i}$ and $D_{i,i+1}$). Thus, we determined the kinetic parameters in our simplified one-dimensional model as;

$$D_{i-1,i} = D_{i,i+1} = 1/2\tau. \quad \text{(S5)}$$

Long-term simulation of the AN3 gradient formation in growing tissue requires four additional parameters: initial setting of cell number, number of source cells that produce the AN3 protein, number of cell divisions and duration of the cell cycle (Fig. S4). We assumed that the duration of the cell cycle was 16 h, based on previous observations (1,2). The other three parameters were determined by analyzing the AN3-3xGFPs distribution (described below).

(4) Numerical simulation for the square FRAP assay

To simulate the square FRAP assay in the leaf upper and lower halves, we determined that 32 and 37 cells, respectively, have uniform relative fluorescence intensity (= 1.0) at an initial state (Fig. S3). We reproduced photobleaching in the square FRAP assay by decreasing the intensity to 0 at $t = 0$ in the 8 and 13 cells located at the centers of the leaf upper and lower halves, respectively. Re-distribution of GFP was investigated by numerical simulation using the experimentally determined kinetic parameter of GFP diffusivity (Fig. 2*C*). We considered that the fluorescence intensity in the cells at tissue boundaries remained constant because of the observation that photobleaching had little effect on the protein concentration in cells located far from the bleached region. We determined that k_{deg} was negligibly small (10^{-10}), as the GFP fluorescence is kept constant without *de novo* production (Fig. S1*A* and S1*B*; Fig. S2*B*). This simulation uniquely determines the value of GFP fluorescence in each cell after calculation.

(5) Numerical simulation for tissue-scale AN3-GFP and AN3-3xGFPs distributions

AN3-3xGFPs is transported solely by dilution through cell proliferation because AN3-3xGFPs is not capable of moving between cells (3,4). Thus, the distribution of AN3-3xGFPs could be approximated by the power-law form;

$$C(x) = F_0 \quad (0 \le x \le x_0), \quad \text{(S6)}$$

$$C(x) = F_0 \cdot x_1/(x - x_0) \quad (x_0 < x). \quad \text{(S7)}$$

A region where cells produce the AN3-3xGFPs but do not proliferate is indicated by x_0. To the best of our knowledge, this x_0 region has not been recognized in the leaf primordia. In addition, the power-law gradient could explain the distribution of AN3-3xGFPs when x_0 is assumed to be zero. F_0 and x_1 denoted the fluorescence intensity and size of source tissue in which cells divide and produce AN3-3xGFPs, respectively. We checked that the time span of *de novo* AN3-GFP production is negligible until 45 min after photobleaching similar to the GFP (Fig. S5*B*). In this model, the AN3-3xGFPs intensity must be related to uniformly spaced values such as cell number from the leaf base (or distance from the leaf base in constant cell-size field) since the AN3-3xGFPs could spread only by growth dilution through cell proliferation as represented by power-law form $C(x)$, which is inversely proportional to the position x. The normalized intensities of AN3-3xGFPs at the fifth and 23rd cells were 1.01 and 0.12, respectively. The ratio of these values was 0.12/1.01, which is ~ $(1/2)^3$, indicating that the concentration of AN3-3xGFPs in the source cell was diluted to $(1/2)^3$ by cell division during the gradient formation. Because there is no report of active proteolysis

of AN3-GFP and AN3-3xGFPs, the ratio indicates that cell division occurs three times during the formation of the AN3-3xGFPs gradient. We determined that the number of source cell $x_1 = 5$, based on the AN3-3xGFPs profile along the leaf proximal-to-distal axis (Fig. 5*C*). This was justified by fitting a curve of the power-law gradient to the experimental data on the AN3-3xGFPs distribution, giving $C(x) = 5.6/x$. Because $C(x_1)$ was ~1.01, we could approximate that x_1 was ~ 5.5. Because our simulation for the AN3-GFP gradient formation required an even number for the source cell number, we used $x_1 = 4$ for the initial condition of simulation. Realistic leaf length at this developmental stage (around 200 μm) could be achieved by this initial condition after uniform cell division at three times (230 μm). These estimations, together with parameters determined above, enabled us to test our model for the AN3-GFP gradient formation without parameter tuning. Thus, we could uniquely determine the value of AN3-GFP intensity in each cell. In contrast to the power-law AN3-3xGFPs gradient, we analyzed the AN3-GFP profile as a function of distance from the leaf base to incorporate cell-size gradient in our simulation model. To compare the experimentally measured and simulated values for the AN3-GFP gradient, cell index *i* was converted to distance from the leaf base based on given cell length. The cell-length distribution was determined essentially based on the experimental observation (Fig. 3*B* and S2*D*). Testing the sensitivity of degradation coefficient in our theoretical model supported the assumption that there is no active proteolysis of AN3-GFP and AN3-3xGFPs in the gradient formation. All parameters are summarized in Tables S1-S3 in the Supplemental Information.

2. Figures S1-S7

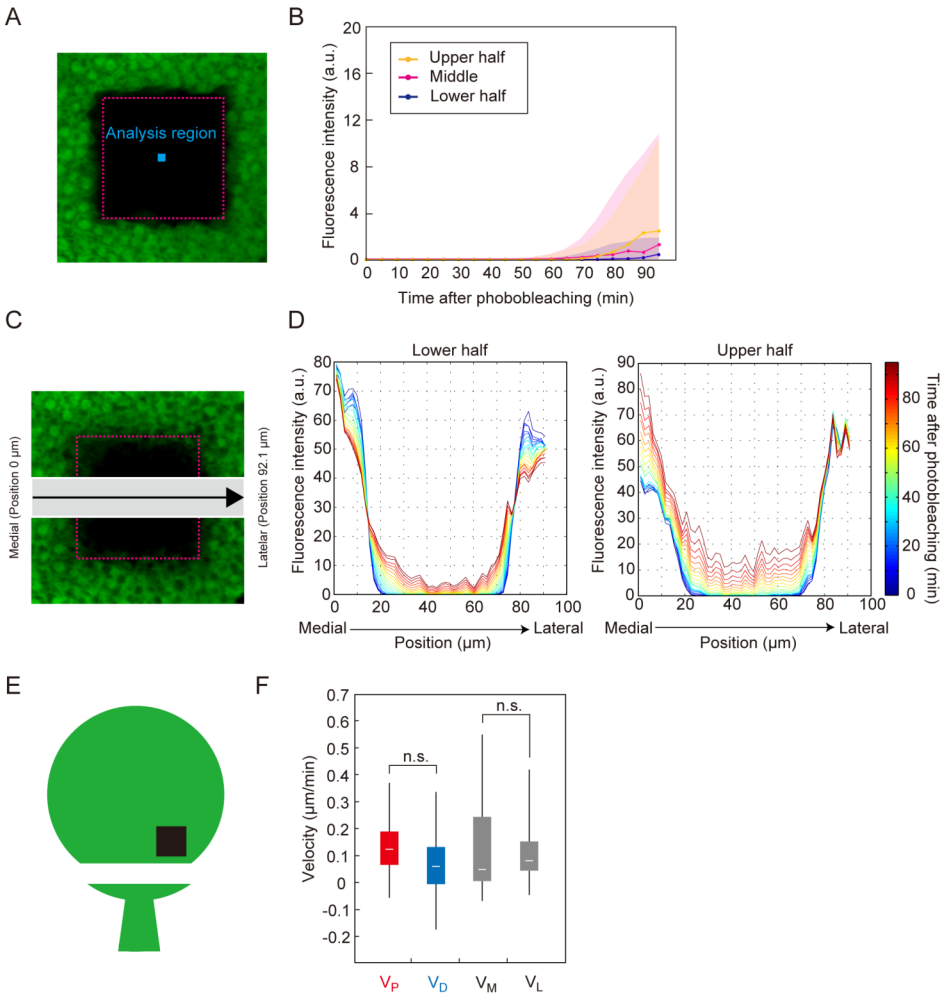

Fig. S1. Characterization of the square FRAP assay. (A and B) Fluorescence from *de novo* synthesized GFP is negligibly small. GFP fluorescence was observed in the center of the ROI [ROI, magenta dashed box; analysis region, blue (1.8 × 1.8 μm)] (A), and was plotted against time after photobleaching (B). The medians (solid line), with 25–75% values of data, are shown (B). (C and D) GFP mobility on a tissue scale is not varied along the leaf medial-to-lateral axis. Constitutively expressed GFP was photobleached (magenta dashed box) in the subepidermal palisade cells of the first leaf primordia in 6-day-old *35S::GFP* transgenic lines. Intensity of GFP fluorescence was scanned along the leaf medial-to-lateral axis [gray stripe (18.4-μm width)] over time (C), and was plotted against the position of the analysis region from medial (0 μm) to lateral (92.1 μm) (D). a.u., arbitrary unit. (E) Schematic illustration of the observed region (black square) in the square FRAP assay using older leaf primordia detached from 10-day-old *35S::GFP* lines. Cell proliferation was arrested in the entire region of the leaf primordia (5). (F) V_D and V_P, velocities of the medial side boundary (V_M) and the lateral side boundary (V_L), respectively, in the lower half of the older leaf primordia. Boxes include the data from 25 to 75% values. Horizontal line in each box shows the median value, where $n = 12$ and n.s. denotes non-significant ($p > 0.05$).

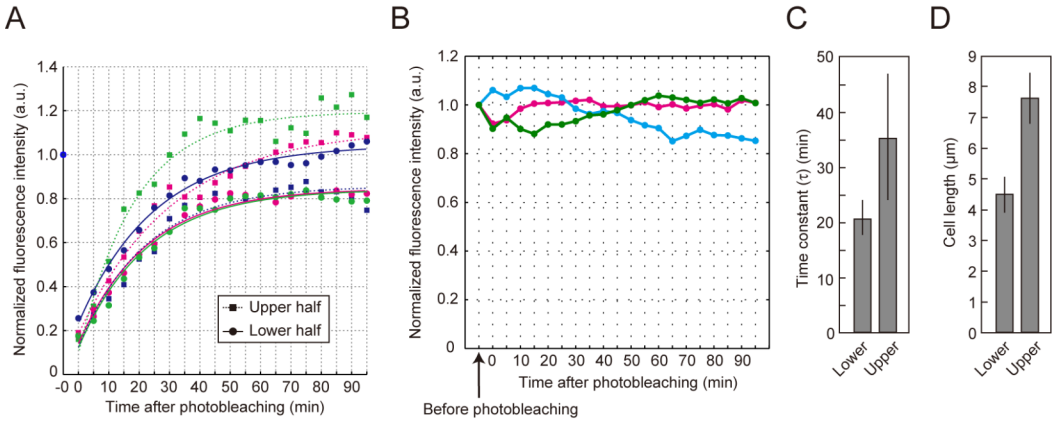

Fig. S2. Recovery kinetics of GFP fluorescence in single-cell FRAP assay from 0 to 95 min after photobleaching; and size of subepidermal cells in the leaf upper and lower halves. (A) Recovery kinetics of GFP fluorescence plotted as a function of time after photobleaching, with -0 being before photobleaching. Squares and circles show GFP fluorescence in the leaf upper and lower halves, respectively. Three representative data, with exponential fits, in each region are shown. Exponential fitting was performed using data from 0 to 95 min after photobleaching. (B) GFP fluorescence intensity in cells adjacent to the targeted cell in single-cell FRAP assay. GFP fluorescence was observed in cells adjacent to the targeted cell and plotted against time before and after photobleaching. Representative data for three independent cells are shown. (C) Time constant (τ) of GFP diffusivity between neighboring cells in the leaf upper and lower halves determined by fitting the recovery profile in (B) with a single exponential recovery. The mean ± s.d. values from seven independent experiments are shown. (D) Cell length is measured in an arbitrary portion of cells in the leaf upper and lower halves. The mean ± s.d. (n = 8–11 cells in each position) are shown.

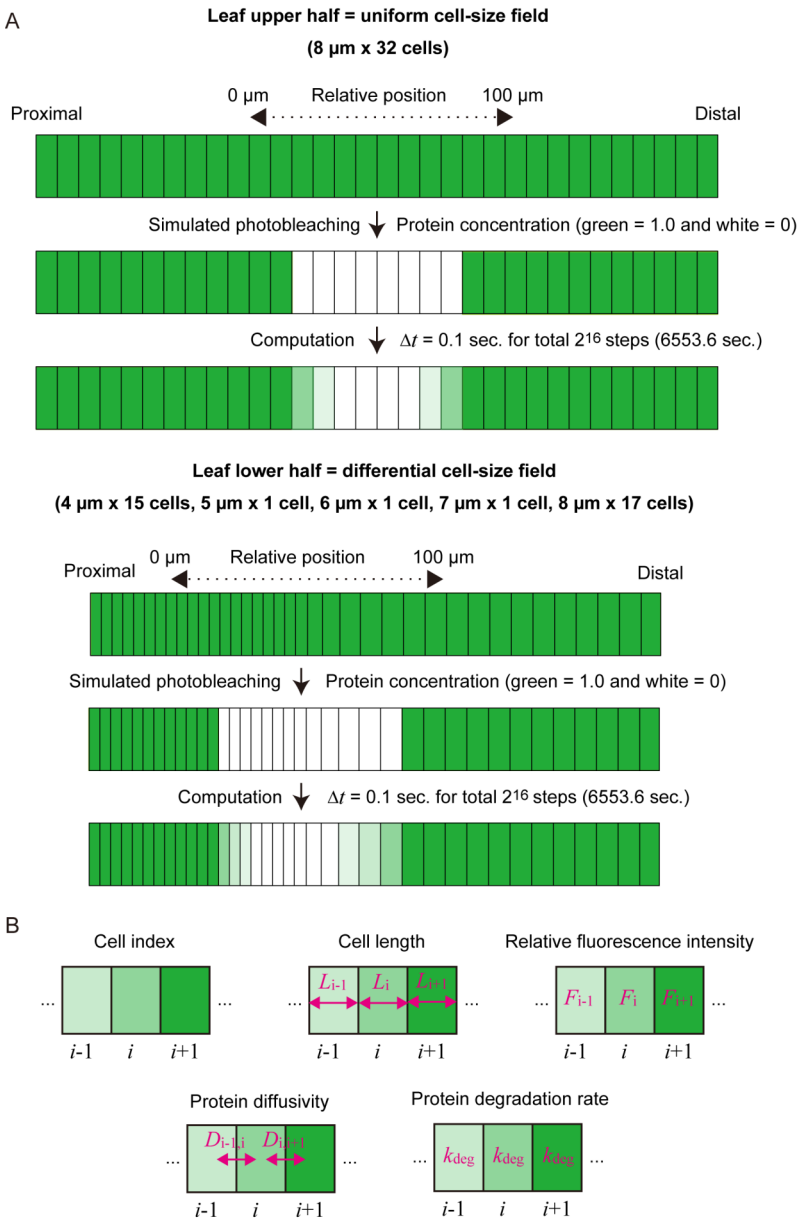

Fig. S3. Diagram of diffusion-based numerical simulation for the square FRAP assay. (A) One-dimensional geometry for simulation of tissue-scale GFP mobility in the square FRAP assay. Uniform and differential cell-size fields were prepared for the leaf upper and lower halves, respectively. Relative fluorescence intensity was then set to zero in a center of analysis area (white region) to reproduce photobleaching, followed by modeling the intensity in each cell based on protein diffusion between neighboring cells. Threshold fluorescence intensity at 0.3 a.u. was used to define the distal and proximal side boundaries. (B) Composition of the numerical simulation for the square FRAP assay. Cell index (i), cell length (L), relative fluorescence intensity (F), protein diffusivity between cells (D), and protein degradation rate (k_{deg}) are used. See *Mathematical models and simulations* section in the Supporting Materials and Methods and Table S1.

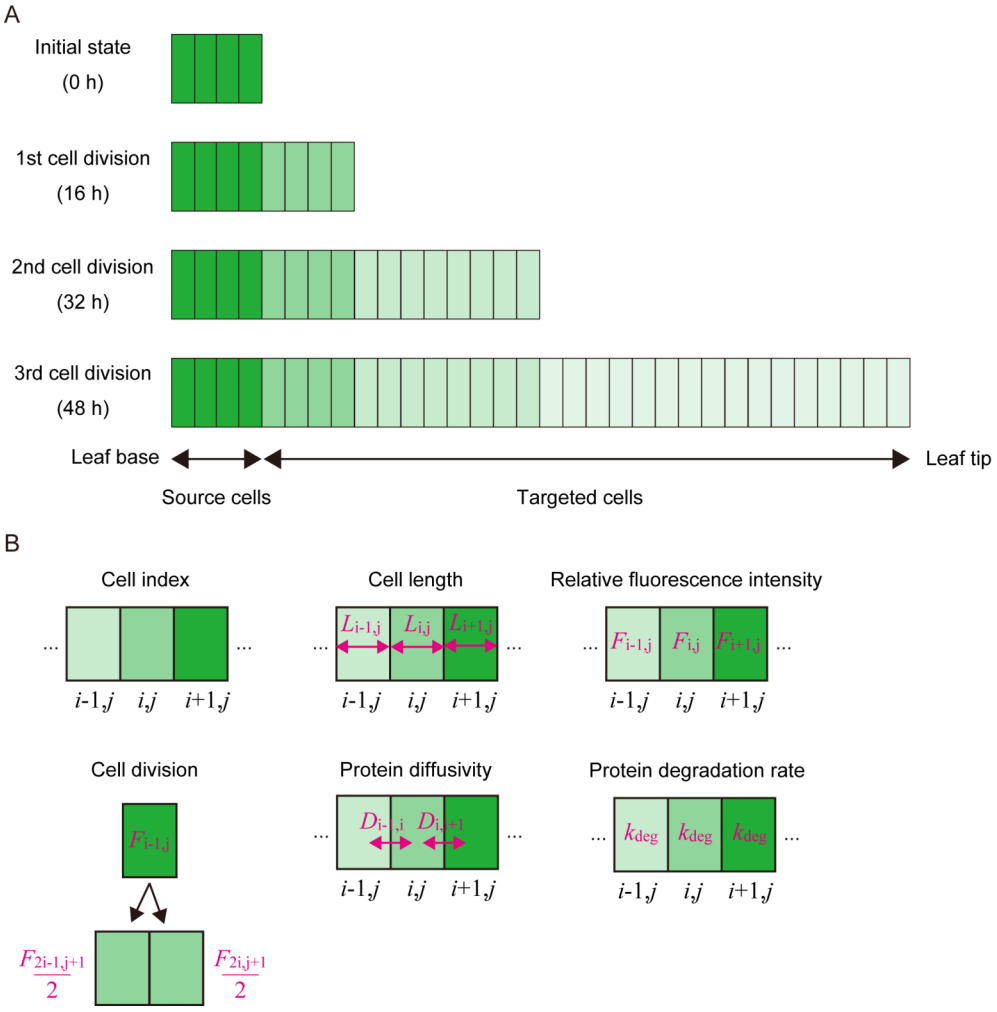

Fig. S4. Diagram of diffusion-based numerical simulation for AN3-GFP gradient formation. (A) Cell-lineage transport of AN3-GFP through targeted cells away from source cells in one-dimensional geometry. We implemented protein diffusion between neighboring cells during this cell-lineage transport for 48 h and analyzed relative fluorescence intensity along the leaf proximal-to-distal axis for simulation of AN3-GFP gradient formation. Initial state for theoretical simulations of the AN3-GFP and the AN3-3xGFPs gradients constitutes of four cells expressing AN3 at a constant level, which was determined by analyzing the AN3-3xGFPs distribution. Distance from leaf base was converted by a given cell length after the simulation to investigate an importance of differential cell-size distribution in the establishment of the AN3-GFP gradient. (B) Composition of our numerical simulation for the AN3-GFP gradient formation. Cell index (i), cell length (L), relative fluorescence intensity (F), cell division, protein diffusivity (D), and protein degradation rate (k_{deg}) were used. See *Mathematical models and simulations* section in the Supporting Materials and Methods and Table S2.

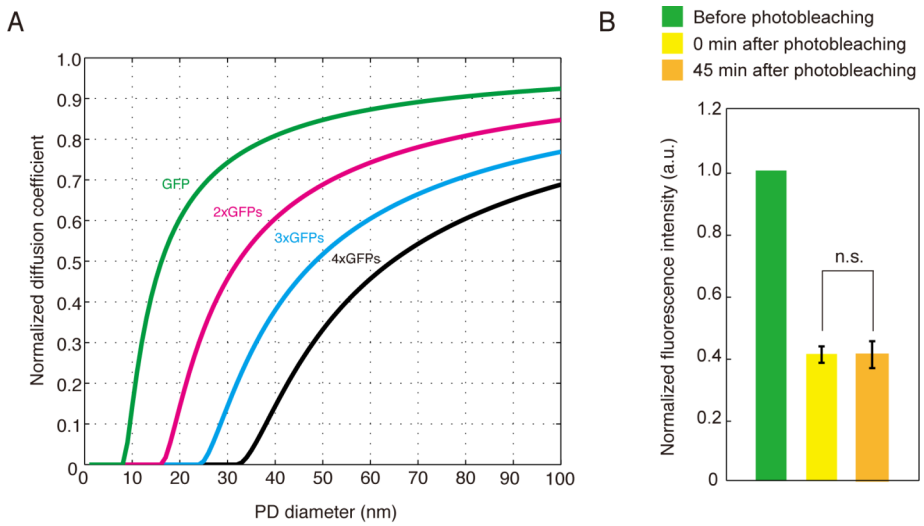

Fig. S5. Characterization of GFP diffusivity and *de novo* AN3-GFP synthesis. (A) Normalized diffusion coefficients of GFP (27 kDa), tandemly fused two GFPs (2xGFPs, 54 kDa), three GFPs (3xGFP, 81 kDa), and four GFPs (4xGFPs, 108 kDa) were estimated by a relationship between diameters of plasmodesmata (p) and spherical molecule (s), based on our previous theoretical model (6). Two parameters are involved in this model; (1) geometric effect of plasmodesmata on the permeability of the molecule (F_1),

$$F_1 = \pi(p/2 - s)^2 / \pi(p/2)^2 = (1 - 2s/p)^2, \quad \text{(S8)}$$

and (2) hydrodynamic drag force on a sphere molecule in the plasmodesmata (F_2) (7). After calculation, the normalized diffusion coefficient was plotted as a function of the plasmodesmata diameter. Because AN3-3xGFPs was not capable of moving between cells in the leaf primordia (3,4) and molecular size of 4xGFPs was close to AN3-3xGFPs (103 kDa), we presumed that the plasmodesmata diameter was less than 33 nm. Diffusivity of 2xGFPs was estimated at 62 % of the GFP diffusivity when we assumed that the plasmodesmata diameter was 30 nm. The characteristic time of 2xGFPs diffusivity between neighboring cells was 40 min under this assumption, in contrast to the GFP diffusivity, which had a characteristic time of 25 min. (B) Fluorescence from *de novo* synthesized AN3-GFP was undetectable during 45 min after photobleaching in the *an3-4/pAN3::AN3-GFP*. Square FRAP assay was performed as essentially described in Figure S1*A*. AN3-GFP fluorescence in a nucleus in a center of ROI was measured before photobleaching, just after photobleaching and 45 min after photobleaching. The mean ± s.d. values from eight independent experiments are shown. Student's *t*-test was performed (n = 8). n.s. denotes non-significant ($p > 0.05$).

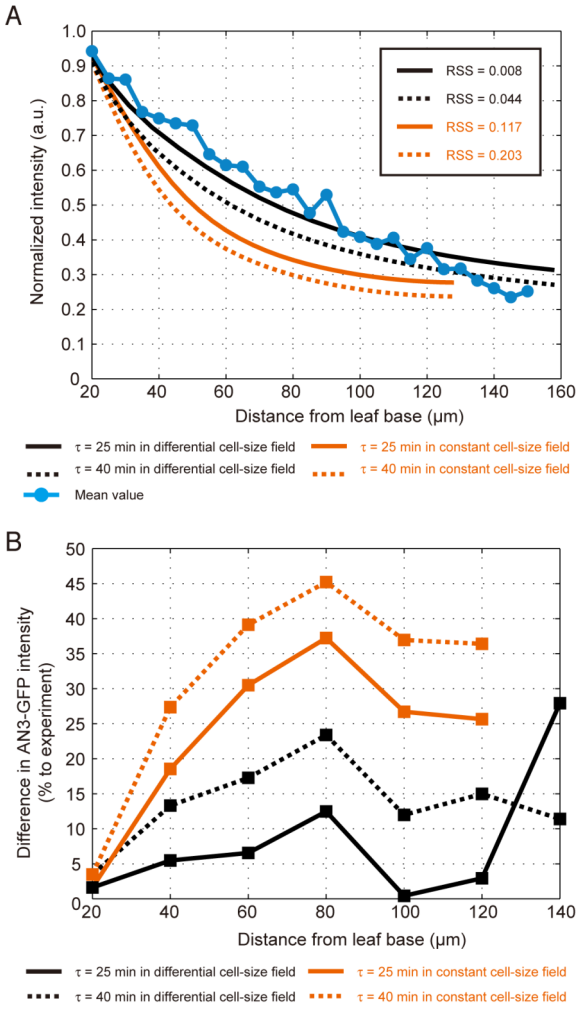

Fig. S6. Numerical simulation of AN3 gradient formation using theoretically predicted diffusivity of 2xGFPs. (A) Experimentally determined mean of AN3-GFP intensity binned by distance from the leaf base at 5-μm intervals (blue dots), simulated curves using diffusivity of GFP (characteristic time = 25 min) with 4-μm constant cell size (orange solid line), and with differential cell size from 4 to 8 μm (black solid line). In addition, we simulated the AN3-GFP gradient using diffusivity of 2xGFPs (characteristic time = 40 min), with 4-μm constant cell size (orange dashed line) and with differential cell size from 4 to 8 μm (black dashed line). (B) Difference in AN3-GFP intensity between simulated and experimentally determined profiles. The differences in simulated curves using diffusivity of GFP (characteristic time = 25 min), with 4-μm constant cell size (orange solid line) and differential cell size from 4 to 8 μm (black solid line), and using diffusivity of 2xGFPs (characteristic time = 40 min) with 4-μm constant cell size (orange dashed line) and with differential cell size from 4 to 8 μm (black dashed line) against experimentally measured values are plotted as a function of distance from the leaf base. Mean deviations were calculated based on the data from 20 to 120 μm from the leaf base. a.u., arbitrary unit. See *Mathematical models and simulations* section in the Supporting Materials and Methods. All parameters used are summarized in Table S3

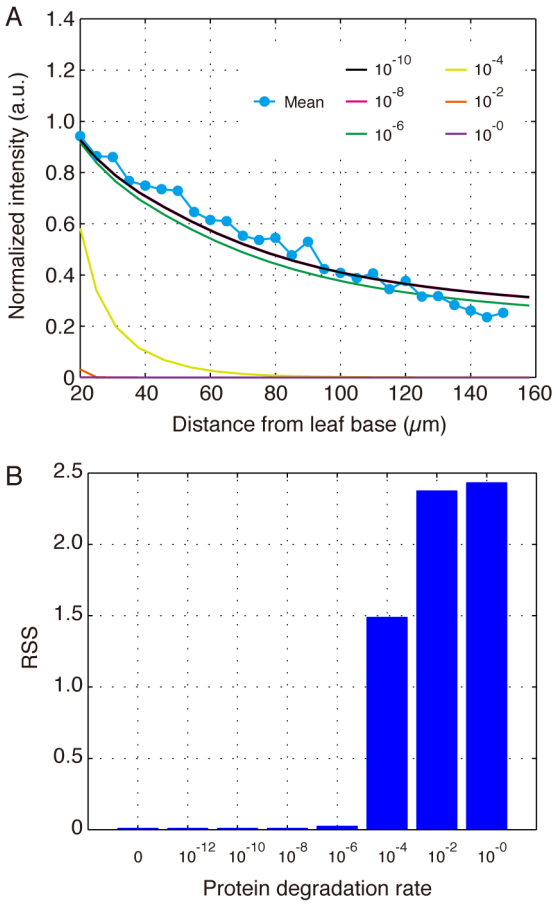

Fig. S7. Sensitivity of AN3 gradient formation to protein degradation. (A) Experimentally determined mean of AN3-GFP intensity binned by distance from the leaf base at 5-μm intervals (blue dots) and simulated curves using various protein degradation coefficients from 10^{-0} to 10^{-10}. Numerical simulation was performed with characteristic time = 25 min and differential cell size from 4 to 8 μm. (B) Difference in AN3-GFP distribution between simulated and experimentally determined profiles represented as residual sum of square.

3. Tables S1-S3

Table S1. Parameters used for the simulation of the square FRAP assay.

Time constant in the leaf upper half	28 min
Time constant in the leaf lower half	22 min
Degradation coefficient	10^{-10} sec^{-1}
Cell size in the leaf upper half	8 μm x 32 cells
Cell size in the leaf lower half	8 μm x 17 cells, 7 μm x 1 cell, 6 μm x 1 cell, 5 μm x 1 cell, 4 μm x 15 cells
Boundary edge intensity	0.3 a.u.

Table S2. Parameters used in the diffusion and growth simulation for the AN3-GFP gradient formation.

Time constant	25 min
Duration of cell cycle	16 hours (1,2)
Cell division	3 times
Source cell number	4 cells
Degradation coefficient	10^{-10} sec^{-1}
Cell size for constant cell-size field	4 μm constant
Cell size for differential cell-size field	4 μm x 1 cell, 5 μm x 1 cell, 6 μm x 1 cell, 7 μm x 1 cell, followed by 8 μm cells

Table S3. Parameters used in the diffusion and growth simulation for the AN3-GFP gradient formation with theoretically estimated 2xGFPs diffusivity.

Time constant	40 min
Duration of cell cycle	16 hours (1,2)
Cell division	3 times
Source cell number	4 cells
Degradation coefficient	10^{-10} sec^{-1}
Cell size for constant cell-size field	4 μm constant
Cell size for differential cell-size field	4 μm x 1 cell, 5 μm x 1 cell, 6 μm x 1 cell, 7 μm x 1 cell, followed by 8 μm cells

4. Movie S1. Recovery of GFP fluorescence in the square FRAP assay.

5. Supporting References

[1] Ichihashi, Y., Kawade, K., Usami, T., Horiguchi, G., Takahashi, T., and Tsukaya, H. 2011. Key proliferative activity in the junction between the leaf blade and leaf petiole of Arabidopsis. Plant Physiol. 157:1151-1162.

[2] Yin, K., Ueda, M., Takagi, H., Kajihara, T., Aki, S.S., Nobusawa, T., Umeda-Hara, C., and Umeda, M. 2014. A dual-color marker system for in vivo visualization of cell cycle progression in Arabidopsis. Plant J. 80:541-552.

[3] Kawade, K., Horiguchi, G., Usami, T., Hirai, M.Y., and Tsukaya, H. 2013. ANGUSTIFOLIA3 signaling coordinates proliferation between clonally distinct cells in leaves. Curr. Biol. 23:788-792.

[4] Kawade, K., Horiguchi, G., and Tsukaya, H. 2010. Non-cell-autonomously coordinated organ size regulation in leaf development. Development. 137:4221-4227.

[5] Ferjani, A., Horiguchi, G., Yano, S., Tsukaya, H. 2007. Analysis of leaf development in *fugu* mutants of Arabidopsis revealed three compensation modes that modulate cell expansion in determinate organs. Plant Physiol. 144:988-999.

[6] Kawade, K., and Tanimoto, H. 2015. Mobility of signaling molecules: the key to deciphering plant organogenesis. J. Plant Res. 128:17-25.

[7] Haberman, W.L., Sayre, R.M. 1958. Motion of rigid and fluid spheres in stationary and moving liquids inside cylindrical tubes. David Taylor Model Basin, Report 1143.